Colloids and Surfaces B: Biointerfaces 227 (2023) 113372

Contents lists available at ScienceDirect

Colloids and Surfaces B: Biointerfaces

journal homepage: www.elsevier.com/locate/colsurfb

Reconsidering the role of albumin towards amorphous calcium phosphate-based calciprotein particles formation and stability from a physico-chemical perspective

Rita Gelli *, Francesca Ridi

Department of Chemistry "Ugo Schiff" and CSGI, University of Florence, via della Lastruccia 3, Sesto Fiorentino, 50019 Florence, Italy

ARTICLE INFO

Keywords:
Calciprotein particles
Amorphous calcium phosphate
Hydroxyapatite
Fetuin-A
Albumin
Proteins

ABSTRACT

The formation of calciprotein particles (CPPs) in serum is a physiological phenomenon fundamental to prevent the rise of ectopic calcifications. CPPs are colloidal hybrid particles made of amorphous calcium phosphate stabilized by a protein, fetuin-A. Since albumin is the most abundant protein present in serum, we aimed at understanding if it plays a synergic action together with fetuin-A towards CPPs formation and stability.

CPPs were prepared using a constant fetuin-A concentration (5 μM) and different concentrations of albumin (0–606 μM). The stability of CPPs, their crystallization and sedimentation were followed *in situ* by combining turbidimetry, precipitation analysis and dynamic light scattering. The morphology was investigated by scanning electron microscopy and cryo-transmission electron microscopy, while crystallinity was inspected by infrared spectroscopy. The effect of albumin on the amount of formed CPPs was also studied, as well as the amount of protein adsorbed on CPPs.

We found that albumin is not able to prolong the lifetime of the amorphous phase, but it is very effective in delaying the sedimentation of CPPs after crystallization. Albumin also significantly decreases the amount and size of CPPs when present in their synthetic medium, likely playing a fundamental role in our organism together with fetuin-A towards the stabilization of CPPs.

1. Introduction

The formation of inorganic nanostructures in living organisms is a fascinating phenomenon in which proteins have a crucial role in modulating the functional properties of the obtained biominerals [1]. Among them, the liver-derived glycoprotein Fetuin-A (Fet-A), known in humans as α2-HS-glycoprotein, circulates in serum at a concentration of ~ 0.8 g/L [2] and is able to bind to amorphous calcium phosphate (ACP) clusters which spontaneously form in plasma and inhibit their growth, thus preventing the surge of ectopic calcifications. The role of Fet-A and other mineral chaperones, such as acidic proteins, is thus fundamental to scavenge calcium ions and nascent calcium phosphate crystals, limiting the ionic supersaturation that would provoke extra-skeletal calcifications [3,4]. Fet-A/ACP complexes are referred to as CPPs (calciprotein particles) and consist of inorganic particles stabilized by Fet-A molecules, that bind calcium phosphate through their acidic residues present in an extended β-sheet in the D1 domain of the protein [1,5]. When in the amorphous state, they are called primary calciprotein particles (CPP1). In time, CPP1 may ripen and crystallize, forming hydroxyapatite-based needle-like structures called secondary CPP (CPP2). Both CPP1 and CPP2 may induce endothelial dysfunction, although primary CPPs cause less deleterious effects than secondary CPPs [6–11]. This biological pathway is especially important for patients affected by kidney diseases, which often suffer from imbalanced homeostasis of phosphate and, in some cases, calcium ions [11,12]. Fet-A has recently been defined as a "mineral chaperone" protecting tissues from calcification and inflammation-related damage [13]; in addition, this glycoprotein displays other biological functions such as the regulation of bone metabolism and the involvement in insulin signaling pathway, also acting as protease inhibitor and inflammatory

Abbreviations: Fet-A, Fetuin-A; ACP, Amorphous calcium phosphate; CPPs, Calciprotein particles; Alb, Albumin; DLS, Dynamic Light Scattering; D_h, Hydrodynamic diameter; SD, Standard Deviation; ICP-OES, Inductively Coupled Plasma Atomic Emission Spectroscopy; FE-SEM, Field Emission - Scanning Electron Microscopy; EDX, Energy Dispersive X-Ray Spectroscopy; TEM, Transmission Electron Microscopy; FT-IR, Fourier Transform - Infrared Spectroscopy.

* Corresponding author.
E-mail address: rita.gelli@unifi.it (R. Gelli).

https://doi.org/10.1016/j.colsurfb.2023.113372
Received 9 December 2022; Received in revised form 3 March 2023; Accepted 24 May 2023
Available online 25 May 2023

mediator [14].

Despite Fet-A is well recognized as the major responsible for the stabilization of CPPs in serum, it has to be considered that hundreds of different types of proteins are present in our blood [15] and among them Albumin (Alb) is by far the most abundant one. Alb circulates in serum at a concentration of 35–50 g/L [16], which is about 50 times higher than that of Fet-A. This protein plays a multifunctional role in blood, as it binds to various endogenous and exogenous molecules and ions, being involved in their transport and homeostasis [17]. Among the ions, Alb is able to bind Ca^{2+} by means of its acidic residues, lowering the concentration of free ions and contributing to the serum calcification inhibition [18]. The efficacy of Alb in preventing serum calcifications is tough controversial: studies from the nineties on the inhibitory capacity of human serum attributed two-thirds of the inhibitory potential to proteins and other macromolecules, Alb accounting for half of the inhibitory effect of the serum proteins [19]. More recent investigations estimated that the contributory fraction of Alb could be as low as ~10% [1]. A series of studies also compared the calcification inhibition potential of Fet-A and Alb: while in 1994 it was shown that, in bovine fetal serum, Alb displays a lower Ca-binding activity than Fet-A [20], Schinke et al. described the calcification propensity of several proteins (Fet-A from different sources, Alb, ovalbumin, calmodulin, lysozyme), and concluded that Fet-A accounts for about half of the serum ability to inhibit mineral precipitation, while Alb had no remarkable effect even at higher concentrations [21]. In terms of CPPs, some works demonstrated that both endogenous and synthetic CPPs contain a substantial fraction of Alb [2,22–24], suggesting that this protein might play a role in their formation and stability. Heiss et al. prepared CPP-like nanoparticles at different Fet-A/Alb concentrations and found that the conversion from CPP1 to CPP2 is driven by Fet-A, whereas Alb only affects the sedimentation process of CPP2, which was monitored for 2 days [2]. They concluded that Fet-A is mainly involved in the stabilization of CPP1 while Alb (and other acidic proteins) stabilize CPP2. A successive paper by Wu et al. studied the effect of Fet-A and Alb towards calcium phosphate mineralization, focusing on the turbidity of cell culture media supplemented with Fet-A/Alb in different conditions, and concluded that both proteins, but in particular Fet-A, exert a strong inhibitory influence on mineral growth and precipitation [25]. Out of note, in their experiment they observed similar results using either human or bovine Fet-A and Alb. A few years later Pasch et al., while developing a nephelometric test to study the calcification propensity of serum [24], observed that Alb has no intrinsic inhibitory effect, but in combination with Fet-A a synergistic inhibitory effect could be observed. In the same work, they conclude that "proteins largely define primary CPP assembly and shape, whereas small molecules largely define primary CPP stability and timing of primary to secondary CPP conversion". The literature presented so far showcases the importance of Alb in the framework of CPPs. Nonetheless, most of the works address the topic from a clinical perspective, without focusing on the colloidal stability and on the nanoscale structure of these inorganic-organic hybrid particles. In particular, the effects of different Alb concentrations on the shape, size, and amount of formed CPPs are of interest, as well as their long-term colloidal stability.

In this work, we investigated the role of Alb on synthetic CPPs formation and stability at constant Fet-A concentration, using 5 μM of Fet-A (1/3 of the physiological one); this concentration was selected in order to evaluate if in a potential pathological situation of low Fet-A levels (associated with an increased risk of mortality in patients suffering from kidney diseases [26,27]), Alb would compensate such deficiency by contributing to CPPs stabilization. Different concentrations of Alb were investigated, from 0 to 606 μM, and the system was analyzed *in situ* at 37 °C by means of turbidimetry, sedimentation and dynamic light scattering, to study the ripening process. The features of the CPP1 formed at different Alb concentrations were thoroughly investigated by combining different analytical approaches including scanning and transmission electron microscopy, infrared spectroscopy and elemental analysis. The obtained results demonstrate that Alb controls both the size and morphology of CPP1 and the stability towards sedimentation of CPP2 dispersions.

2. Materials and methods

2.1. Materials

$CaCl_2$ (purity > 93.0%), NaCl (purity > 99.5%), $Na_2HPO_4{\cdot}12\ H_2O$ (purity > 99.0%), Fetuin from fetal bovine serum (Type III, n° F3385, M_w 48,400 g/mol) and Bovine Serum Albumin (n° A9418, M_w 66,000 g/mol) were purchased from Sigma Aldrich. Tris(hydroxymethyl)aminomethane (TRIS, purity > 99.7%) was obtained from Fluka while HCl 37% from Carlo Erba Reagents. Milli-Q water (resistivity 18.2 MΩ·cm) was used in all the experiments.

2.2. CPPs preparation

CPPs were prepared upon mixing of aqueous solutions containing dissolved salts and proteins. TRIS-HCl buffer 50 mM was prepared by dissolving 0.303 g of TRIS in 50 mL of Milli-Q water. The pH (pH meter 7 + with DHS electrode, XS instruments) was lowered from the initial value of ~10 to 7.40 by dropwise addition of HCl 1 M. Two precursors' solutions, A and B, were prepared: solution A was made by dissolving $CaCl_2$ (0.022 g, 20 mM) and NaCl (0.164 g, 280 mM) in 10 mL of the TRIS-HCl 50 mM solution, while solution B was obtained by dissolving 0.043 g of $Na_2HPO_4{\cdot}12\ H_2O$ (12 mM) in 10 mL of TRIS-HCl 50 mM. Fet-A (2.91 mg) was dissolved in 3 mL of solution B, yielding to solution C ([Fet-A]= 20 μM), whereas Alb (160 mg) was dissolved in 1 mL of solution B, resulting in solution D ([Alb]= 2424 μM). All solutions were heated at 37 °C, and samples were obtained upon mixing them according to the volumes reported in Table 1. Solutions B, C and D were mixed and added to solution A. The final concentrations in the 2 mL volume samples were [Ca^{2+}]= 10 mM, [Na^+]= 140 mM, [phosphate]: 6 mM, [Fet-A]= 5 μM and [Alb] from 0 to 606 μM. The obtained dispersions were incubated at 37 °C and, when needed, 1 mL aliquots were collected at selected times and centrifuged (Neya 16 R, REMI, A6–50 rotor) at 12,000 rpm for 5 min, then washed with 1 mL of water and centrifuged again in the same conditions. The supernatant was discarded, and the precipitate was frozen in liquid nitrogen and lyophilized at − 55 °C and 30 mTorr for 24 h (VirTis benchtop freeze-dryer).

2.2.1. Addition of albumin after CPP formation

As a comparison, CPPs were also prepared by adding Alb after 2 min from the mixing of precursors' solutions. In this case, 1.45 mg of Fet-A were dissolved in 3 mL of solution B, and heated at 37 °C. This solution was mixed with 3 mL of solution A. After 2 min, 1 mL of the reacting solution was added to 0.99 mg, 7.52 mg and 29.99 mg of Alb in order to

Table 1
Amounts of solutions used for samples preparation (total volume: 2 mL) and final concentrations of proteins in each sample. Solution A: $CaCl_2$ 20 mM and NaCl 280 mM in TRIS-HCl 50 mM; Solution B: $Na_2HPO_4{\cdot}12\ H_2O$ 12 mM in TRIS-HCl 50 mM; Solution C: Fet-A 20 μM in solution B; Solution D: Alb 2424 μM in solution B.

Sample	Solution A	Solution B	Solution C	Solution D	[Fet-A]	[Alb]
F5_A0	1 mL	500 μL	0.5 mL	-	5 μM	0 μM
F5_A2.5	1 mL	498 μL	0.5 mL	2 μL	5 μM	2.5 μM
F5_A10	1 mL	492 μL	0.5 mL	8 μL	5 μM	10 μM
F5_A20	1 mL	483 μL	0.5 mL	17 μL	5 μM	20 μM
F5_A76	1 mL	437 μL	0.5 mL	63 μL	5 μM	76 μM
F5_A303	1 mL	250 μL	0.5 mL	250 μL	5 μM	303 μM
F5_A606	1 mL	-	0.5 mL	500 μL	5 μM	606 μM

obtain samples F5_A10_post, F5_A76_post, F5_A303_post. After 3 min from Alb addition, the dispersions were centrifuged at 12,000 rpm for 5 min, washed with 1 mL of water, centrifuged again and eventually freeze-dried.

2.2.2. Synthesis of CPPs at lower calcium concentration

As a reference, F5_A0 was prepared using a lower amount of Ca^{2+} with respect to the synthesis described in Section 2.2. 21.53 mg of $Na_2HPO_4{\cdot}12\ H_2O$ were dissolved in 5 mL of 50 mM TRIS-HCl buffer at pH 7.4, together with 2.45 mg of Fet-A (solution B). 164 mg of NaCl were dissolved in 10 mL of 50 mM TRIS-HCl buffer (solution A): this solution was divided in two 5 mL aliquots, in which 8.88 mg and 6.66 mg of $CaCl_2$ were dissolved, leading to a $[Ca^{2+}]$= 16 mM and 12 mM, respectively. CPPs were obtained by mixing at 37 °C 1 mL of both solutions A with 1 mL of solution B, obtaining a final calcium concentration in the reacting medium of 8 mM and 6 mM. Both samples were collected by means of centrifugation after 5 min of reaction and treated as described in Section 2.2.

2.3. Characterization techniques

2.3.1. Turbidimetry

Turbidimetry measurements were performed with a Cary 3500 spectrophotometer (Agilent). Samples were prepared as described in Section 2.2, and immediately after mixing the dispersions were quickly placed in PMMA cuvettes and loaded in the spectrophotometer. The measurement was carried out at 37 °C for 16 h by recording the absorbance at 400 nm every 2 min. An integration time of 0.020 s and a bandwidth of 1 nm were used to collect the absorbance data. 50 mM solution of TRIS-HCl was used for baseline subtraction.

2.3.2. Sedimentation

The sedimentation process of CPP dispersions was monitored visually, by collecting photos of the samples in time. Samples were prepared as described in Section 2.2, placed in PMMA cuvettes and stored in an oven at 37 °C. Photos were analyzed with the software ImageJ, converting them in 8 bit and performing auto-contrast operation to make the darkest spot (photos background) as pixel value= 0 and the whitest as 255. The grey value, *i.e.*, pixel value, from the top to the bottom of the cuvette was measured, in order to monitor the sedimentation of CPPs (see a sketch in Fig. S1 in the Supplementary Material).

2.3.3. Dynamic Light Scattering (DLS)

DLS measurements were performed at 37 °C with a Particle Size Analyzer 90 Plus (Brookhaven Instruments) equipped with a 635 nm laser. Immediately after the preparation, samples were placed in a cuvette and the autocorrelation functions were acquired by averaging 10 runs of 10 s each. Measurements were carried out after 5 min, 15 min, 30 min, 45 min, 60 min, 75 min, 90 min, 105 min, 120 min and 180 min from the beginning of the reaction. The autocorrelation functions were processed with the Contin algorithm developed by Provencher [28,29] with the 9kpsdw software package from Brookhaven Instruments. The obtained size distribution curves for the hydrodynamic diameters (D_h) were fitted with the software IgorPro, using a gaussian function (see Eq. 1):

$$y = y_0 + A\exp\left[-\left(\frac{x - x_0}{width}\right)^2\right] \quad (1)$$

where x_0 represents the D_h and *width* is $SD\sqrt{2}$ (SD=standard deviation).

2.3.4. Inductively Coupled Plasma Atomic Emission Spectroscopy (ICP-OES)

The amount of unreacted calcium during CPP formation was measured by means of an Inductively Coupled Plasma Atomic Emission Spectrometer (ICP-OES). CPPs were prepared as described in Section 2.2. After 5 min of reaction at 37 °C, the dispersions were centrifuged at 12,000 rpm for 5 min and the supernatant was collected. Calcium concentration was determined in triplicate by means of an Agilent 720-ES ICP-OES equipped with a pneumatic nebulizer and a cyclonic spray chamber. 1.0 ppm of Ge was used as an internal standard to correct any matrix effect. The calibration lines were obtained by preparing the standard solutions starting from commercial standards certified at 1000 ppm. The line used for Ca determination was 422.673 nm whereas the one used for Ge was at 209.426 nm. After each measurement, the system was washed with a 2% HNO_3 solution. The obtained amount of Ca was compared with that initially present in the reacting solution, and results were expressed as % of Ca left in the supernatant after the reaction.

2.3.5. Field Emission - Scanning Electron Microscopy (FE-SEM) coupled with Energy Dispersive X-Ray Spectroscopy (EDX)

FE-SEM micrographs were collected using a Zeiss ΣIGMA FE-SEM (Carl Zeiss Microscopy GmbH). The freeze-dried samples were placed on aluminum stubs using conductive tape. The accelerating voltage was 2 kV, the sample-detector distance ~2 mm and the aperture 10 μm. Images were acquired with an In-Lens detector. The size distributions were obtained measuring the diameter of ~200 particles *per* sample, using the software ImageJ. The obtained histograms were fitted with the software IgorPro, using a gaussian function (see Eq. 1). EDX analysis was carried out using an accelerating voltage of 10 kV, a sample-detector distance ~8 mm and an aperture of 60 μm. The Ca/P ratios were obtained as average ± standard deviation of three different sites *per* sample.

2.3.6. Cryo-Transmission Electron Microscopy (Cryo-TEM)

Cryo-TEM images were collected using a Glacios™ microscope (Thermo Fisher Scientific) operating at 200 kV and equipped with a FEI Falcon 3 detector operating in counting mode. A volume of 3 μL of particles dispersions reacted for 5 min was deposited on glow discharged (PELCO easiGlow™ Glow Discharge Cleaning System) Quantifoil R2/2 holey carbon films on 300 Cu Mesh + 2 nm C grids and plunged frozen into liquid ethane using an FEI VitRobot Mark IV (Thermo Fisher Scientific). Excess liquid was removed by blotting for 2 s (blot force 0) using filter paper under 100% humidity and 10 °C.

2.3.7. Fourier Transform - Infrared Spectroscopy (FT-IR)

FT-IR spectra were collected in transmission mode using an Agilent Cary 670 spectrometer. KBr pellets were prepared by mixing 1 mg of freeze-dried sample and 100 mg of KBr (FT-IR grade, Sigma Aldrich). Spectra were collected in the 4000–400 cm^{-1} range, using a resolution of 2 cm^{-1} and 128 scans. A KBr pellet was used for the background subtraction.

2.3.8. Elemental analysis CHNS

The amount of C in the freeze-dried samples collected after 5 min of reaction was determined by means of a FlashSmart Elemental Analyzer CHNS/O (Thermoscientific) operating with a dynamic flash combustion of the sample and a Thermal Conductivity Detector (TCD).

3. Results and discussion

The effect of Alb towards CPPs formation and stability was initially studied *in situ* at 37 °C by means of turbidimetry, which is a well-suited technique to monitor the formation and ripening of CPPs [30]. The obtained curves up to 2 h are shown in Fig. 1A, while the process monitored up to 16 h is shown in Fig. S2. In samples F5_A0 and F5_A2.5 we observe that the absorbance rises very slowly for about 30 min, then it abruptly increases reaching a plateau, and eventually drops to ~ 0. These stages are compatible with the initial formation of CPP1, followed by their ripening with the formation of CPP2 and finally their precipitation (see a sketch of the different stages in Fig. S3A). In the presence of

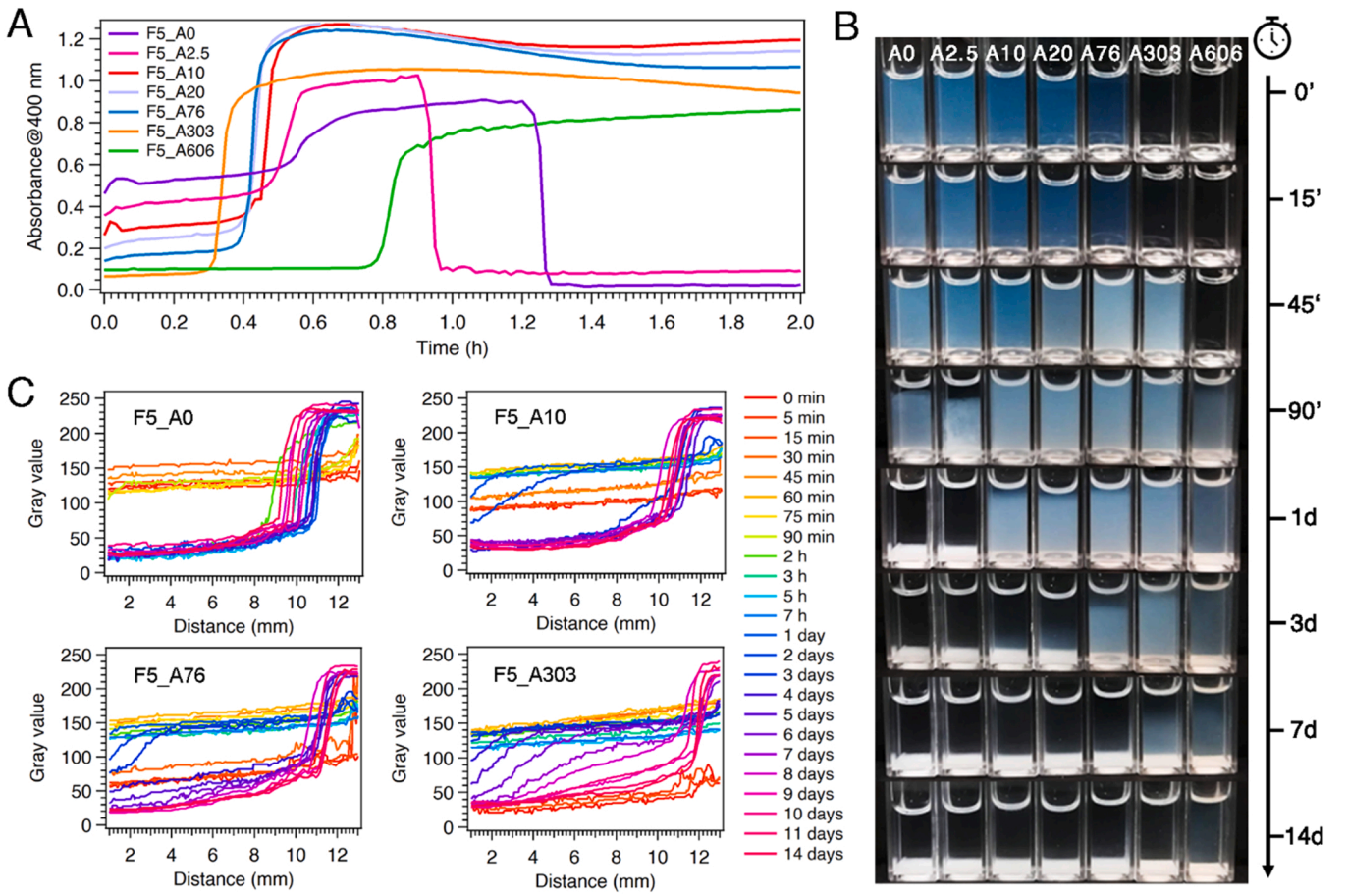

Fig. 1. A) Turbidimetry curves at 37 °C of the samples under investigation (see the profile up to 16 h in Fig. S1). B) Photos of the different samples as a function of time incubated at 37 °C. C) Gray values profiles as a function of distance from the interphase of photos in B, at different incubation times (see Fig. S5 for an explanation of the process).

intermediate Alb concentrations (from sample F5_A10 to F5_A76), the ripening occurs on similar timescales than without Alb, but no precipitation is observed up to 16 h. The onset times of the ripening transition, calculated as the intersection point between the tangents to the curves in the stage I and II (see Fig. S3B), are reported in Table 2, and confirm that the conversion process from CPP1 to CPP2 occurs on similar time scales irrespectively of Alb concentration, at least up to [Alb]= 76 μM. Sample F5_A303, in fact, ripens faster than samples at lower Alb concentration, while for F5_A606 the process is remarkably slower (see Fig. 1A and Table 2). Interestingly, all samples but F5_A606 show an initial absorbance value which is inversely proportional to Alb concentration (see Table 2 and Fig. S4). Since the amount of scattering and absorption depends on the size of the particles and their concentration in the suspension [31], we can infer that the presence of Alb leads to the formation of CPPs which are either smaller or less concentrated (or both).

The results obtained from turbidimetry were compared with the visual observation of the samples in time, shown in Fig. 1B. Immediately after mixing, the optical density of the dispersions decreases with the increase of Alb concentration, consistently with data reported Fig. S4. The abrupt increase in absorbance first occurs in sample F5_A303, as already pointed out from the analysis of the onset times in Table 2. While turbidimetry allows for the monitoring of the systems for a limited amount of time, from samples observation we can monitor the sedimentation process up to weeks. Interestingly, while samples F5_A0 and F5_A2.5 begin their precipitation after about one hour, samples at higher Alb concentration are stable up to 1 day and complete the precipitation process in several days. Alb is thus very effective in slowing down the sedimentation process of the colloidal dispersion, as the precipitation

Table 2
Parameters obtained from turbidimetry, DLS and FE-SEM/EDX. The latter two techniques refer to samples collected after 5 min. For DLS, the SD associated to D_h is obtained from the width of the gaussian fit of the size distribution curves obtained by the Contin analysis of the autocorrelation functions. For FE-SEM, the errors associated to the diameter and SD result from the Gaussian fit of the size distribution curves (see Section 2.3.6). For EDX, results are average ± SD of three sites *per* sample.

Sample	Turbidimetry		DLS	FE-SEM/EDX		
	Onset time (min)	Absorbance at t = 0	D_h ± SD (nm)	Diameter (nm)	SD (nm)	Ca/P
F5_A0	29 min	0.46	166 ± 41	69.7 ± 2.0	17.9 ± 3.5	1.20 ± 0.01
F5_A2.5	28 min	0.36	156 ± 16	57.1 ± 1.3	20.0 ± 1.8	1.22 ± 0.03
F5_A10	27 min	0.26	133 ± 44	43.5 ± 0.3	8.1 ± 0.4	1.26 ± 0.02
F5_A20	25 min	0.20	125 ± 44	42.5 ± 0.5	10.1 ± 0.7	1.24 ± 0.05
F5_A76	25 min	0.14	180 ± 35	43.3 ± 0.6	10.7 ± 0.8	1.22 ± 0.03
F5_A303	19 min	0.07	6 ± 2, 39 ± 12, 136 ± 28	21.7 ± 0.7	4.6 ± 1.1	1.26 ± 0.05
F5_A606	47 min	0.10	8 ± 1, 356 ± 97	-	-	-

process is inversely proportional to Alb concentration. Sample F5_A606 shows a different behavior with respect to the other samples, as the solution is transparent up to ~45 min, then it turns slightly turbid and maintains a constant turbidity up to about 7 days, when the precipitation process slowly begins.

The evolution of the sedimentation process was followed by developing a method for the images analysis, described in Section 2.3.2, which takes advantage of the evaluation of the gray value of the image along the sample volume. As depicted in Fig. S5, when the dispersion is stable (*i.e.*, the sample color is homogeneous), the gray values profile consists of a flat line. When the precipitation begins, the gray values of the portion of sample that does not any longer contain particles are lower (meaning closer to black), while the portion that contains the precipitate is characterized by higher gray values. The less abrupt is the rise along the sample profile from low to high gray value, the more gradual is the precipitation. When the precipitation is complete, the transition from low to high gray values has a sigmoidal profile. Photos at different times were analyzed, and the gray values as a function of the distance from the interphase of representative samples are reported in Fig. 1C (the plots for all samples are given in Fig. S6 in the Supplementary Material). For sample F5_A0 we can clearly see that the precipitation process occurs quite abruptly within few hours. In the presence of Alb, the precipitation process occurs more slowly, and it is more gradual, in particular for F5_A303.

To sum up, we observed that Alb does not markedly affect the onset time of the transition from CPP1 to CPP2, but it noticeably increases the colloidal stability of CPP2 against sedimentation; moreover, the initial turbidity of the dispersions is inversely proportional to Alb concentration, suggesting the formation of smaller or less concentrated particles in the medium. These results confirm some previously reported findings on the ability of Alb to delay CPP2 sedimentation [2], although at different concentrations and sedimentation times.

The size of the particles formed in the reacting medium was analyzed *in situ* by means of DLS. The obtained autocorrelation functions were fitted with the Contin method, and the obtained size distribution curves are given in Fig. S7. The D_h after 5 min reported in Table 2 was obtained as the center of the gaussian curve that fits the size distribution histograms in Fig. S7. Taking into account the SD associated to the D_h values, samples from F5_A0 to F5_A76 show a similar hydrodynamic diameter and are characterized by a single size distribution curve, as shown in Fig. S7. Samples F5_A303, in contrast, shows three size distribution curves: the first one, centered at 6 nm, is compatible with the presence of free albumin molecules in solution [32,33], while the other two are centered at 39 nm and 136 nm, respectively. Sample F5_A606 shows two size distribution curves, the first one is again compatible with free albumin in solution and the second one suggests the presence of very large and polydisperse objects. DLS experiment was carried out for 3 h, and it was possible to observe that for samples from F5_A0 and F5_A76 the average size of the particles in solution increases in the timeframe from 30 to 45 min, in agreement with turbidimetry onset times. For F5_A303, the size increases in the 15–30 min range, whereas for F5_A606, this occurs after about 1 h, again in agreement with turbidimetry. By combining turbidimetry and DLS results it is possible to conclude that the increase in turbidity observed in time is related to an increase in the size of the particles in solution, reasonably due to the CPP1 to CPP2 transition. Alb affects the ripening time only when at high concentrations.

The effect of Alb towards the structure of CPP1 was characterized by analyzing samples aged for 5 min. The amount of CPPs which initially form in the medium is also important to unravel Alb effect. In fact, even if this protein appears ineffective in delaying the conversion from CPP1 to CPP2, it might have an effect in diminishing the amount of CPPs formed in serum. As already stated, the initial turbidity of the dispersions (see Fig. 1B and Fig. S4) appears inversely proportional to Alb content in the medium. The amount of formed particles after 5 min of reaction was assessed with two different approaches. On the one hand, the amount of particles collected after centrifugation, washing and freeze-drying was weighted and the calculated mg/mL were plotted as a function of Alb concentration in Fig. 2A (green dots, left y axis). For this test, samples were prepared as described in Section 2.2, but the total volume was scaled-up to 10 mL, in order to obtain an amount of solid that could be reliably weighted with an analytical balance. In F5_A606, no precipitate is formed within the first 5 min, so this sample was not accounted for in the analysis. We observe that the amount of particles that can be recovered after centrifugation is inversely proportional to Alb content in the medium. This was confirmed by assessing the amount of Ca^{2+} left in the supernatant after centrifugation by means of ICP-OES (see Section 2.3.4), which increases with the increase of Alb in the system (see Fig. 2A, light blue triangles, right y axis). Out of note, the % of residual Ca^{2+} in the solution for sample F5_A0 (56%) well agrees with previous investigations from the literature [34]. These two separate experiments demonstrate that Alb diminishes the number of CPPs that initially form in the system.

The morphology of the particles collected after 5 min of reaction was analyzed by means of FE-SEM, and the micrographs are reported in Fig. 3, along with the size distribution curves in Fig. S8. Also in this case, sample F5_A606 could not be analyzed due to the lack of particles precipitation upon centrifugation after 5 min of reaction. All samples consist of spherical nanoparticles; their average size is reported in Table 2, while the diameter as a function of Alb concentration is shown in Fig. 2B. Notably, the presence of Alb significantly decreases the size of the CPPs in a concentration-dependent fashion. It is worth mentioning that DLS did not show a significant difference in sample's D_h: this could

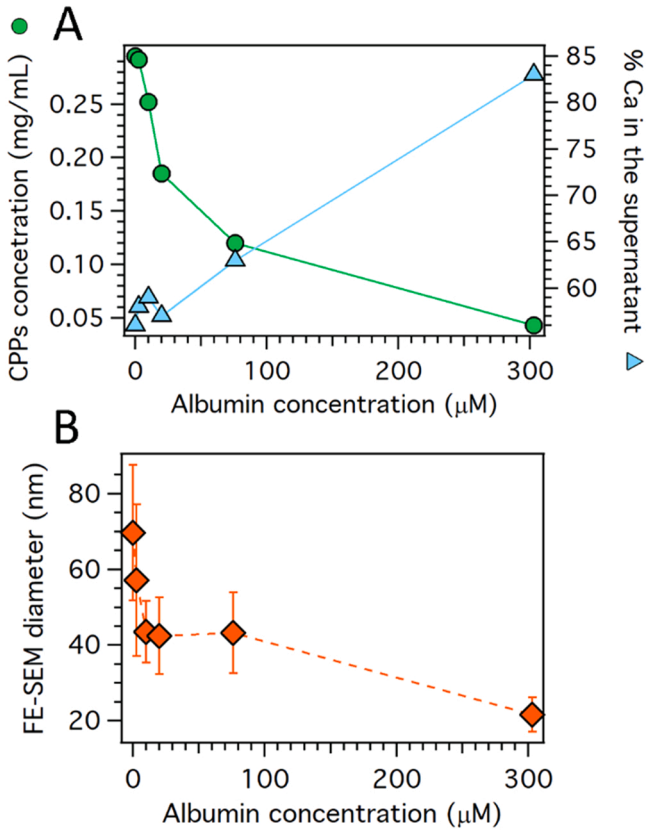

Fig. 2. A) On the left, concentration of CPPs (mg/mL) as a function of Alb concentration, obtained from the weight of the precipitate (green dots). On the right, % of Ca left in the supernatant after centrifugation, obtained by ICP-OES (light blue triangles). B) Plot of the CPPs diameter as obtained by FE-SEM micrographs (see Table 2) as a function of Alb concentration. Error bars represent the SD obtained from the Gaussian fittings of the size distribution curves given in Fig. S8.

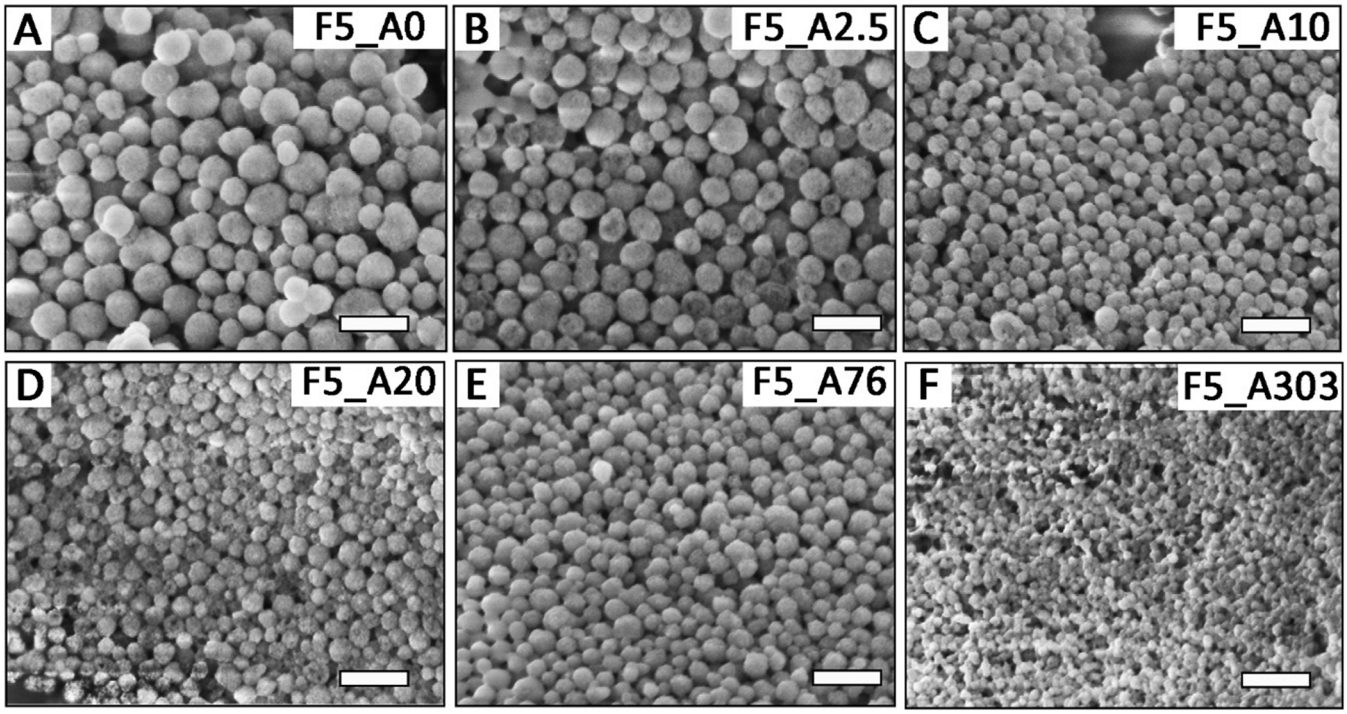

Fig. 3. FE-SEM micrographs of CPPs collected after 5 min. The scale bar for all images is 200 nm.

be related to the fact that the D_h reflects the size of the inorganic core together with its hydration shell, which may comprise protein molecules and their hydration water. Moreover, during the freeze-drying procedure carried out before SEM, the protein shell might collapse. Thus, it is possible that by increasing Alb concentration in solution the size of the inorganic core diminishes and, at the same time, the amount of protein adsorbed on its surface increases.

The Ca/P ratio of the particles, measured by means of EDX analysis coupled with SEM experiments, is compatible with amorphous calcium phosphate [35] and is not affected by the concentration of Alb in the reacting medium (see Table 2 and Fig. S9).

In order to understand if Alb effect towards CPPs size is restricted to its presence during the initial stages of particles formation, we carried out an additional experiment by preparing CPPs only in the presence of Fet-A 5 μM, and we added different amounts of Alb (10, 76 and 303 μM) after 2 min from the beginning of the reaction (see further details on this procedure in Section 2.2.1). The micrographs of the obtained CPPs together with the size distribution curves are given in Fig. S10 in the Supplementary Material. The comparison of the particle's diameters prepared with the two synthetic protocols at a given Alb concentration reported in Fig. S11 shows that when Alb is added after the initial CPPs formation, no significant variation in CPP size is observed, suggesting that Alb has to be present during the initial nucleation of the particles in order to display an effect on their size.

Bearing in mind that Alb is believed to interact with calcium ions at pH 7.4 [36], we speculated that its effect might be related to a decrease of the active Ca^{2+} concentration in the reacting medium. To assess this hypothesis, we replicated the synthetic protocol for sample F5_A0, using a total Ca^{2+} concentration of 8 mM and 6 mM instead of 10 mM (see Section 2.2.2). The obtained micrographs and the size distribution curves are reported in Fig. S12 and show a slight decrease in the diameter of the particles when the concentration of calcium is lowered (57 ± 6 nm for the sample prepared with $[Ca^{2+}]$=6 mM and 62 ± 13 nm for $[Ca^{2+}]$=8 mM with respect to 70 ± 18 nm for F5_A0). Nevertheless, considering the width of the size distributions, this effect is not significant. We can thus speculate that Alb effect in decreasing the size of CPPs is reasonably not related to a Ca^{2+}-sequestration effect but rather to an adsorption on CPPs surface that limits the growth of the nanoparticle.

The morphology of CPP1 at different Alb concentrations was further investigated by means of Cryo-TEM measurements. With respect to conventional TEM, here samples preparation does not involve a slow drying step of the dispersion on the sample grid which might cause the unwanted crystallization of the unstable CPP1. Representative micrographs are given in Fig. 4. In all samples we observe spherical nanoparticles compatible with CPPs morphology [37]. In the presence of Alb, CPPs appear more separated one from the other, and their size is on average smaller than sample F5_A0. Moreover, in samples containing Alb, it is also possible to observe very small objects (few nm) in the background, compatible with free protein molecules deposited on the sample grid. It is worth commenting on the surface of CPPs, which is rough and wrinkled in all samples, especially in those containing Alb. We hypothesized that this morphology might be due to the adsorption of proteins on the surface of ACP. As a comparison, we imaged a sample prepared in the absence of proteins and vitrified immediately after mixing calcium and phosphate precursors' solutions (see Fig. S13). The obtained nanoparticles also display a rough surface, suggesting that the amorphous nature of calcium phosphate is responsible for the rough morphology. Nonetheless, on this length scale particles obtained without proteins are more similar to sample F5_A0 rather than to those containing Alb, suggesting that this protein influences the morphology of the single CPP particles.

FT-IR spectroscopy was used to acquire information on the nature of the inorganic phases constituting the samples. The spectra of the particles collected after 5 min are shown in Fig. 5, while the spectra of the pristine proteins are given in Fig. S14. All samples show the main peaks characteristic of amorphous calcium phosphate, namely the broad band at 3700–2700 cm^{-1} due to O-H stretching, the peak at ~1650 cm^{-1} corresponding to water O-H bending, the strong peak in the 1200–920 cm^{-1} region related to P-O antisymmetric stretching (ν_3) and the peak at 565 cm^{-1} due to P-O antisymmetric bending (ν_4) [38]. The broad and featureless nature of those peaks testifies the amorphous nature of the samples [39]. In addition, signals diagnostic of the proteins can also be distinguished in all spectra, in particular the C-H stretching

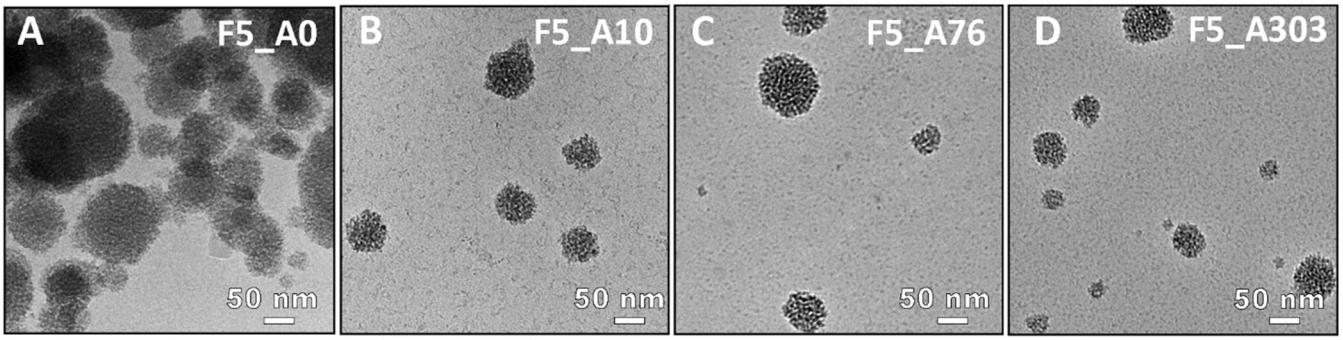

Fig. 4. Cryo-TEM micrographs of samples A) F5_A0, B) F5_A10, C) F5_A76, D) F5_A303 vitrified after 5 min from the beginning of the synthesis.

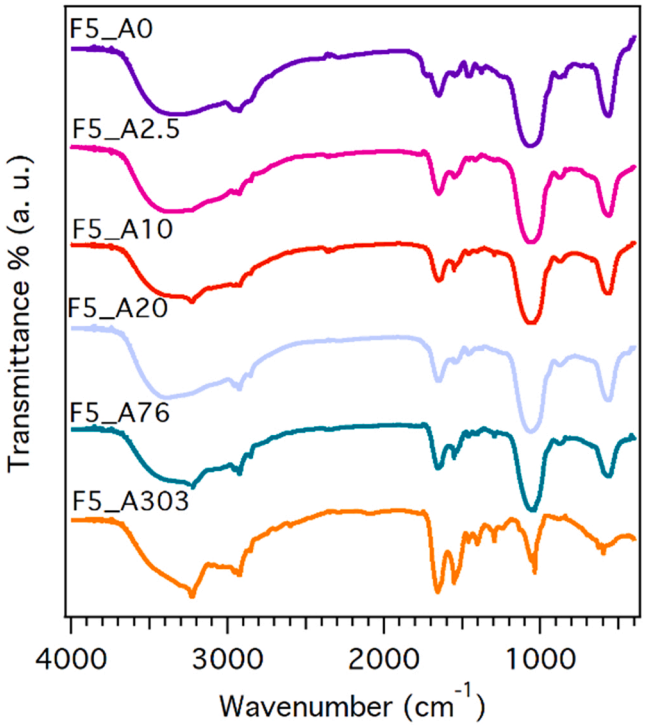

Fig. 5. FT-IR spectra of the samples at different Alb concentration collected after 5 min. The curves have been offset along the y axis for display purposes.

signal below 3000 cm^{-1} and amide II peaks at ~1540 cm^{-1}, mainly evident in sample F5_A303. Fet-A and Alb, as expected, do not show any significant difference in their spectrum, preventing the identification of one or the other component in the hybrid CPPs. Moreover, the overlap between Amide I peak (commonly used for deconvolutions to determine proteins' secondary structure [40]) and water bending of amorphous calcium phosphate prevents a deeper analysis of the structure of the proteins adsorbed on the nanoparticles.

The amount of proteins adsorbed on CPPs was quantified by means of CHNS analysis (see Section 2.3.8). The results for our samples and for the pure proteins are reported in Table S1 in the Supplementary Material. Knowing the amount of C in Fet-A and Alb is essential to relate the amount of C in the samples to the amount of proteins in CPPs. As expected, both proteins show a similar elemental composition in terms of N, C and H %. Alb has a higher % of S with respect to Fet-A, reasonably due to the higher amount of cysteine and methionine in its sequence [41, 42]. We estimated the total amount of proteins present in CPP samples considering an average C content for both proteins as 45%, and the results are given in Fig. 6A and Table S1. Interestingly, the amount of proteins in CPP samples is constant (about 15% wt) up to sample F5_A10, and significantly increases when Alb concentration is above 20 μM. This might suggest that at low Alb concentrations its amount adsorbed on CPPs is negligible, despite displaying an effect on the nanoparticles size (see Fig. 2B). This is supported by the observation of S % in the samples, which is the same for samples F5_A0, F5_A2.5 and F5_A10 (see Table S1). Samples F5_A20, F5_A76 and F5_A303, on the contrary, show a slightly larger amount of S, confirming that in such samples also Alb is present in CPPs. One can also calculate the % of proteins incorporated in CPPs with respect to those initially present in solution during the synthesis. The results, shown in Fig. 6B and Table S1, reveal that in Sample F5_A0 only about 18% of the Fet-A initially present in the reacting medium is adsorbed on CPPs, while as the total amount of proteins in the reacting media increases, the % is significantly reduced.

Concerning the effect of Alb towards CPP2, we characterized by means of FE-SEM the particles after 6 h of reaction, so after the ripening process and before precipitation (except for F5_A0 and F5_A2.5, which precipitate after about 1 h). The obtained micrographs, reported in Fig. S15, show that Alb does not affect the morphology of CPP2, as all samples display the features typical of poorly-crystalline hydroxyapatite [30]. Given that also by means of DLS no significant difference in the CPP2 size was detected after the ripening (see Fig. S7), we concluded that the only effect of Alb on CPP2 is to slow down their sedimentation (as already discussed), not affecting their morphology, size, and crystallinity.

Sample F5_A606 behaves differently from the other samples. We already mentioned that it was not possible to collect any precipitate upon centrifugation after 5 min, suggesting that CPP1 formation did not occur in these conditions. The dispersion remains transparent for ~45 min (see Fig. 1), resulting then in a poorly turbid suspension, which very slowly precipitates. We collected the product formed after 1 h and 6 h, and FE-SEM investigation did not reveal any difference in terms of sample morphology (see Fig. S16). We can therefore conclude that in these conditions CPP1 formation and transition to CPP2 does not occur, as after an initial induction period poorly crystalline hydroxyapatite directly forms, not being mediated by an amorphous transient precursor. It is interesting to point out that [Alb]= 606 μM (*i.e.,* ~40 g/L) is a value within the physiological range [2] and, despite that, the results show that in this case we do not obtain the physiological CPP1 to CPP2 pathway. It is though important to recall Alb multi-functional role in our blood, where it binds endogenous and exogenous molecules, transports ions in the circulation, acts as a toxic waste carrier, as an anti-oxidant and as scavenger for reactive oxygen and nitrogen species [16]. Keeping that in mind, we can hypothesize that the amount of Alb free to interact with CPPs would be way lower than the one resulting from the nominal concentration.

4. Conclusions

The aim of this work was to unravel the effect of Alb towards the formation and stability of endogenous-like CPPs from a physico-

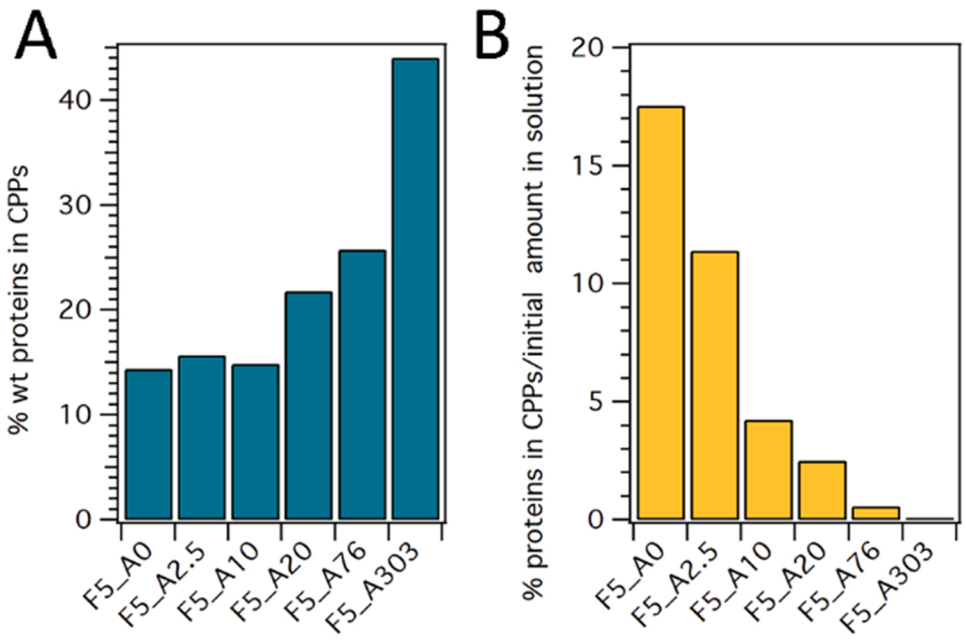

Fig. 6. Results of CHNS analysis: A) % of proteins present in each sample calculated as the ratio between the weight of the proteins and the weight of the CPPs; B) % of proteins present in CPPs with respect to the initial amount present in the reacting solution.

chemical perspective. CPPs formation in blood is a physiological phenomenon relevant to the preservation of ionic homeostasis and to prevent the surge of ectopic calcifications [11]. The excessive formation of CPP1 and especially their ripening to CPP2 might though result in pathological situations [5]. Understanding how these processes occur in our body and which are the factors involved in their formation and stability is thus of paramount importance to better understand their role and find strategies to preserve their functioning. Since Alb is the most abundant protein in serum [16], here we report on its impact towards CPPs formation and stability. CPP samples were prepared at constant Fet-A concentration (5 μM) and with different amounts of Alb, up to the physiological concentration. The ripening process was studied in situ by means of turbidimetry and DLS. We observed that up to [Alb]= 76 μM, the ripening time from CPP1 to CPP2 is independent on Alb concentration, suggesting that the protein is not able to slow down the amorphous-to-crystalline transition. With 303 μM of protein the process is accelerated, while when [Alb]= 606 μM it is delayed. Interestingly, the observation of the sedimentation process carried out for several days revealed a remarkable colloidal stability of the CPP2 system when increasing Alb concentration. This is in agreement with a previous report in the literature that showed that, even at different concentrations from those used in our work, the presence of Alb slows down the sedimentation process [2]. DLS showed that no significant difference in the hydrodynamic diameter of the objects present in solution was observed at different Alb concentrations, also due to the polydispersity of the samples. We focused our attention on the features of the CPP1 at different Alb concentration, finding that the amount of particles that forms in the reacting medium is inversely proportional to Alb concentration. Therefore, even if Alb is not able to stabilize the amorphous phase of CPP1, it is able to diminish the number of particles that form, which would also be important in the context of preventing unwanted accumulations of calcium phosphates in the body. Out of note, Alb is also able to reduce the size of CPP1, as we observed from both scanning and transmission electron microscopy investigations. The amount of proteins present in CPPs was also determined, showing that Alb is included in the CPPs only when high concentrations are present in the reacting medium.

In conclusion, it is evident that Alb is not able to compensate for an eventual lack of Fet-A, as the action mechanism of the two proteins towards CPPs is different: while increasing Fet-A concentration results in a delay of the ripening time from CPP1 to CPP2 and of the CPP2 sedimentation [30], Alb leads to smaller CPP1 and decreases their amount in solution, also stabilizing CPP2 against sedimentation. Even if the importance of Fet-A in the formation and stability of CPPs is unquestionable, our work corroborates the idea that Alb takes place in this biologically relevant phenomenon. As a step forward, biomimetic media more closely resembling the in vivo environment could be envisaged, either using proteins extracted from human serum or studying CPPs formation in systems including other biorelevant proteins and molecules.

CRediT authorship contribution statement

Rita Gelli: Conceptualization, Methodology, Formal analysis, Investigation, Writing - Original Draft, Writing - Review & Editing, Visualization., **Francesca Ridi:** Conceptualization, Methodology, Resources, Writing - Review & Editing, Funding acquisition.

Declaration of Competing Interest

The authors declare that they have no known competing financial interests or personal relationships that could have appeared to influence the work reported in this paper.

Data Availability

Data will be made available on request.

Acknowledgements

CSGI consortium, MUR PRIN - 2017249YEF and MIUR-Italy (“Progetto Dipartimenti di Eccellenza 2018–2022″ allocated to Department of Chemistry “Ugo Schiff”) are acknowledged for financial support. Access to the Thermoscientific FlashSmart Elemental Analyzer CHNS/O facility and to the FloCEN facility of the Department of Chemistry ‘Ugo Schiff’ of the University of Florence is gratefully acknowledged. Prof. Mirko Severi from the University of Florence is acknowledged for ICP-OES measurements and Dr. Annalisa Guerri from the FloCEN-University of

Florence is acknowledged for the cryo-TEM measurements.

Appendix A. Supporting information

Supplementary data associated with this article can be found in the online version at doi:10.1016/j.colsurfb.2023.113372.

References

[1] D.C. Bassett, L.M. Grover, F.A. Müller, M.D. McKee, J.E. Barralet, Serum protein controlled nanoparticle synthesis, Adv. Funct. Mater. 21 (2011) 2968–2977, https://doi.org/10.1002/adfm.201100320.

[2] A. Heiss, T. Eckert, A. Aretz, W. Richtering, W. van Dorp, C. Schäfer, W. Jahnen-Dechent, Hierarchical role of fetuin-A and acidic serum proteins in the formation and stabilization of calcium phosphate particles, J. Biol. Chem. 283 (2008) 14815–14825, https://doi.org/10.1074/jbc.M709938200.

[3] O. Söhnel, F. Grases, Supersaturation of body fluids, plasma and urine, with respect to biological hydroxyapatite, Urol. Res. 39 (2011) 429–436, https://doi.org/10.1007/s00240-011-0387-5.

[4] M.M.X. Cai, E.R. Smith, S.G. Holt, The role of fetuin-A in mineral trafficking and deposition, Bone Rep. 4 (2015) 672, https://doi.org/10.1038/bonekey.2015.39.

[5] C.N. Silaghi, T. Ilyés, A.J. Van Ballegooijen, A.M. Crăciun, Calciprotein particles and serum calcification propensity: hallmarks of vascular calcifications in patients with chronic kidney disease, J. Clin. Med 9 (2020) 1287, https://doi.org/10.3390/jcm9051287.

[6] A.G. Kutikhin, E.A. Velikanova, R.A. Mukhamadiyarov, T.V. Glushkova, V. V. Borisov, V.G. Matveeva, L.V. Antonova, D.E. Filip'ev, A.S. Golovkin, D. K. Shishkova, A.Y. Burago, A.V. Frolov, V.Y. Dolgov, O.S. Efimova, A.N. Popova, V. Y. Malysheva, A.A. Vladimirov, S.A. Sozinov, Z.R. Ismagilov, D.M. Russakov, A. A. Lomzov, D.V. Pyshnyi, A.K. Gutakovsky, Y.A. Zhivodkov, E.A. Demidov, S. E. Peltek, V.F. Dolganyuk, O.O. Babich, E.V. Grigoriev, E.B. Brusina, O. L. Barbarash, A.E. Yuzhalin, Apoptosis-mediated endothelial toxicity but not direct calcification or functional changes in anti-calcification proteins defines pathogenic effects of calcium phosphate bions, Sci. Rep. 6 (2016) 27255, https://doi.org/10.1038/srep27255.

[7] D. Shishkova, A. Lobov, B. Zainullina, V. Matveeva, V. Markova, A. Sinitskaya, E. Velikanova, M. Sinitsky, A. Kanonykina, Y. Dyleva, A. Kutikhin, Calciprotein particles cause physiologically significant pro-inflammatory response in endothelial cells and systemic circulation, Int. J. Mol. Sci. 23 (2022) 14941, https://doi.org/10.3390/ijms232314941.

[8] D.K. Shishkova, E.A. Velikanova, L.A. Bogdanov, M.Y. Sinitsky, A.E. Kostyunin, A. V. Tsepokina, O.V. Gruzdeva, A.V. Mironov, R.A. Mukhamadiyarov, T. V. Glushkova, E.O. Krivkina, V.G. Matveeva, O.N. Hryachkova, V.E. Markova, Y. A. Dyleva, E.V. Belik, A.V. Frolov, A.R. Shabaev, O.S. Efimova, A.N. Popova, V. Y. Malysheva, R.P. Kolmykov, O.G. Sevostyanov, D.M. Russakov, V.F. Dolganyuk, A.K. Gutakovsky, Y.A. Zhivodkov, A.S. Kozhukhov, E.B. Brusina, Z.R. Ismagilov, O. L. Barbarash, A.E. Yuzhalin, A.G. Kutikhin, Calciprotein particles link disturbed mineral homeostasis with cardiovascular disease by causing endothelial dysfunction and vascular inflammation, Int. J. Mol. Sci. 22 (2021) 12458, https://doi.org/10.3390/ijms222212458.

[9] D. Shishkova, V. Markova, M. Sinitsky, A. Tsepokina, E. Velikanova, L. Bogdanov, T. Glushkova, A. Kutikhin, Calciprotein particles cause endothelial dysfunction under flow, Int. J. Mol. Sci. 21 (2020) 8802, https://doi.org/10.3390/ijms21228802.

[10] D. Shishkova, E. Velikanova, M. Sinitsky, A. Tsepokina, O. Gruzdeva, L. Bogdanov, A. Kutikhin, Calcium phosphate bions cause intimal hyperplasia in intact aortas of normolipidemic rats through endothelial injury, Int. J. Mol. Sci. 20 (2019) 5728, https://doi.org/10.3390/ijms20225728.

[11] A. Pasch, W. Jahnen-Dechent, E.R. Smith, Phosphate, calcification in blood, and mineral stress: the physiologic blood mineral buffering system and its association with cardiovascular risk, Int. J. Nephrol. 2018 (2018) 1–5, https://doi.org/10.1155/2018/9182078.

[12] K.M. Hill Gallant, D.M. Spiegel, Calcium balance in chronic kidney disease, Curr. Osteoporos. Rep. 15 (2017) 214–221, https://doi.org/10.1007/s11914-017-0368-x.

[13] S. Rudloff, W. Jahnen-Dechent, U. Huynh-Do, Tissue chaperoning—the expanded functions of fetuin-A beyond inhibition of systemic calcification, Pflüg. Arch. Eur. J. Physiol. 474 (2022) 949–962, https://doi.org/10.1007/s00424-022-02688-6.

[14] E. Chekol Abebe, Z. Tilahun Muche, A. Behaile T/Mariam, T. Mengie Ayele, M. Mekonnen Agidew, M. Teshome Azezew, E. Abebe Zewde, T. Asmamaw Dejenie, M. Asmamaw Mengstie, The structure, biosynthesis, and biological roles of fetuin-A: A review, Front. Cell Dev. Biol. 10 (2022), 945287, https://doi.org/10.3389/fcell.2022.945287.

[15] J. Cui, Q. Liu, D. Puett, Y. Xu, Computational prediction of human proteins that can be secreted into the bloodstream, Bioinformatics 24 (2008) 2370–2375, https://doi.org/10.1093/bioinformatics/btn418.

[16] A.M. Merlot, D.S. Kalinowski, D.R. Richardson, Unraveling the mysteries of serum albumin—more than just a serum protein, Front. Physiol. 5 (2014) 299, https://doi.org/10.3389/fphys.2014.00299.

[17] T. Peters Jr., All About Albumin: Biochemistry, Genetics, and Medical Applications, Academic Press,, 1995.

[18] A.G. Kutikhin, L. Feenstra, A.E. Kostyunin, A.E. Yuzhalin, J.-L. Hillebrands, G. Krenning, Calciprotein particles: balancing mineral homeostasis and vascular pathology, Arterioscler. Thromb. Vasc. Biol. 41 (5) (2021) 1607–1624, https://doi.org/10.1161/ATVBAHA.120.315697.

[19] J. Garnett, P. Dieppe, The effects of serum and human albumin on calcium hydroxyapatite crystal growth, Biochem. J. 266 (1990) 863–868.

[20] M. Suzuki, H. Shimokawa, Y. Takagi, S. Sasaki, Calcium-binding properties of fetuin in fetal bovine serum, J. Exp. Zool. 270 (1994) 501–507, https://doi.org/10.1002/jez.1402700603.

[21] T. Schinke, C. Amendt, A. Trindl, O. Pöschke, W. Müller-Esterl, W. Jahnen-Dechent, The serum protein α2-HS Glycoprotein/Fetuin Inhibits Apatite Formation in Vitro and in Mineralizing Calvaria Cells: a possible role in mineralization and calcium homeostasis, J. Biol. Chem. 271 (1996) 20789–20796, https://doi.org/10.1074/jbc.271.34.20789.

[22] J. Martel, D. Young, A. Young, C.-Y. Wu, C.-D. Chen, J.-S. Yu, J.D. Young, Comprehensive proteomic analysis of mineral nanoparticles derived from human body fluids and analyzed by liquid chromatography–tandem mass spectrometry, Anal. Biochem. 418 (2011) 111–125, https://doi.org/10.1016/j.ab.2011.06.018.

[23] E.R. Smith, T.D. Hewitson, E. Hanssen, S.G. Holt, Biochemical transformation of calciprotein particles in uraemia, Bone 110 (2018) 355–367, https://doi.org/10.1016/j.bone.2018.02.023.

[24] A. Pasch, S. Farese, S. Gräber, J. Wald, W. Richtering, J. Floege, W. Jahnen-Dechent, Nanoparticle-based test measures overall propensity for calcification in serum, J. Am. Soc. Nephrol. 23 (2012) 1744–1752, https://doi.org/10.1681/ASN.2012030240.

[25] C.-Y. Wu, J. Martel, D. Young, J.D. Young, Fetuin-A/albumin-mineral complexes resembling serum calcium granules and putative nanobacteria: demonstration of a dual inhibition-seeding concept, PLoS One 4 (2009), e8058, https://doi.org/10.1371/journal.pone.0008058.

[26] M. Ketteler, P. Bongartz, R. Westenfeld, J.E. Wildberger, A.H. Mahnken, R. Böhm, T. Metzger, C. Wanner, W. Jahnen-Dechent, J. Floege, Association of low fetuin-A (AHSG) concentrations in serum with cardiovascular mortality in patients on dialysis: a cross-sectional study, Lancet 361 (2003) 827–833, https://doi.org/10.1016/S0140-6736(03)12710-9.

[27] Z. Zhou, Y. Ji, H. Ju, H. Chen, M. Sun, Circulating fetuin-A and risk of all-cause mortality in patients with chronic kidney disease: a systematic review and meta-analysis, Front. Physiol. 10 (2019) 966, https://doi.org/10.3389/fphys.2019.00966.

[28] S.W. Provencher, A constrained regularization method for inverting data represented by linear algebraic or integral equations, Comput. Phys. Commun. 27 (1982) 213–227, https://doi.org/10.1016/0010-4655(82)90173-4.

[29] S.W. Provencher, CONTIN: A general purpose constrained regularization program for inverting noisy linear algebraic and integral equations, Comput. Phys. Commun. 27 (1982) 229–242, https://doi.org/10.1016/0010-4655(82)90174-6.

[30] R. Gelli, V. Pucci, F. Ridi, P. Baglioni, A study on biorelevant calciprotein particles: Effect of stabilizing agents on the formation and crystallization mechanisms, J. Colloid Interface Sci. 620 (2022) 431–441, https://doi.org/10.1016/j.jcis.2022.04.025.

[31] T. Kourti, Turbidimetry in Particle Size Analysis. Encycl. Anal. Chem, John Wiley & Sons, Ltd,, 2006, https://doi.org/10.1002/9780470027318.a1517.

[32] E. Velichko, S. Makarov, E. Nepomnyashchaya, G. Dong, Molecular aggregation in immune system activation studied by dynamic light scattering, Biology 9 (2020) 123, https://doi.org/10.3390/biology9060123.

[33] B. Lorber, F. Fischer, M. Bailly, H. Roy, D. Kern, Protein analysis by dynamic light scattering: methods and techniques for students, Biochem. Mol. Biol. Educ. 40 (2012) 372–382, https://doi.org/10.1002/bmb.20644.

[34] A. Heiss, V. Pipich, W. Jahnen-Dechent, D. Schwahn, Fetuin-A is a mineral carrier protein: small angle neutron scattering provides new insight on fetuin-a controlled calcification inhibition, Biophys. J. 99 (2010) 3986–3995, https://doi.org/10.1016/j.bpj.2010.10.030.

[35] S.V. Dorozhkin, Synthetic amorphous calcium phosphates (ACPs): preparation, structure, properties, and biomedical applications, Biomater. Sci. 9 (2021) 7748–7798, https://doi.org/10.1039/D1BM01239H.

[36] K.O. Pedersen, Binding of calcium to serum albumin II. Effect of pH via competitive hydrogen and calcium ion binding to the imidazole groups of albumin, Scand. J. Clin. Lab. Invest. 29 (1972) 75–83, https://doi.org/10.3109/00365517209081058.

[37] A.E. Schantl, M.E. Ivarsson, J.-C. Leroux, Investigational pharmacological treatments for vascular calcification, Adv. Ther. 2 (2019) 1800094, https://doi.org/10.1002/adtp.201800094.

[38] R. Gelli, M. Scudero, L. Gigli, M. Severi, M. Bonini, F. Ridi, P. Baglioni, Effect of pH and Mg2+ on amorphous magnesium-calcium phosphate (AMCP) stability, J. Colloid Interface Sci. 531 (2018) 681–692, https://doi.org/10.1016/j.jcis.2018.07.102.

[39] C. Drouet, Apatite formation: why it may not work as planned, and how to conclusively identify apatite compounds, BioMed. Res. Int. 2013 (2013), 490946, https://doi.org/10.1155/2013/490946.

[40] H. Yang, S. Yang, J. Kong, A. Dong, S. Yu, Obtaining information about protein secondary structures in aqueous solution using Fourier transform IR spectroscopy, Nat. Protoc. 10 (2015) 382–396, https://doi.org/10.1038/nprot.2015.024.

[41] K. Siriwardana, A. Wang, M. Gadogbe, W.E. Collier, N.C. Fitzkee, D. Zhang, Studying the effects of cysteine residues on protein interactions with silver nanoparticles, J. Phys. Chem. C Nanomater. Interfaces 119 (2015) 2910–2916, https://doi.org/10.1021/jp512440z.

[42] C. Wang, I. Lascu, A. Giartosio, Bovine serum fetuin is unfolded through a molten globule state, Biochemistry 37 (1998) 8457–8464, https://doi.org/10.1021/bi9723010.